



Papers published in *Ocean Science Discussions* are under
open-access review for the journal *Ocean Science*

High resolution modelling of the North Icelandic Irminger Current (NIIC)

K. Logemann and I. H. Harms

Centre for Marine and Climate Research, Institute for Oceanography, University of Hamburg,
Bundesstrasse 53, 20146 Hamburg, Germany

Received: 14 June 2006 – Accepted: 23 June 2006 – Published: 1 August 2006

Correspondence to: I. H. Harms (harms@ifm.uni-hamburg.de)

NIIC modelling

K. Logemann and
I. H. Harms

[Title Page](#)

[Abstract](#)

[Introduction](#)

[Conclusions](#)

[References](#)

[Tables](#)

[Figures](#)

◀

▶

◀

▶

[Back](#)

[Close](#)

[Full Screen / Esc](#)

[Printer-friendly Version](#)

[Interactive Discussion](#)

EGU

Abstract

The northward inflow of Atlantic Water through Denmark Strait – the North Icelandic Irminger Current (NIIC) – is simulated with a numerical model of the North Atlantic and Arctic Ocean. The model uses the technique of adaptive grid refinement which allows 5 a high spatial resolution (1 km horizontal, 10 m vertical) around Iceland. The model is used to assess time and space variability of volume and heat fluxes for the years 1997–2003. Passive tracers are applied to study origin and composition of NIIC water masses.

The NIIC originates from two sources: the Irminger Current, flowing as part of the 10 sub-polar gyre in 100–500 m depth along the Reykjanes Ridge and the shallow Icelandic coastal current, flowing eastward on the south Icelandic shelf. The ratio between the deep and shallow branch is 0.7/0.2 Sv. The NIIC continues as a warm and saline branch northward through Denmark Strait where it entrains large amounts of polar water due to the collision with the southward flowing East Greenland Current. Tracer 15 model results indicate that north of Denmark Strait at Hornbanki section (at 21°30' W from 66°40' N to 67°30' N), the NIIC is composed of 43% water masses of Atlantic origin (AW) originating from the south and 57% entrained polar or Arctic water masses (PW) coming from the north. After passing Denmark Strait, the NIIC follows the coast line north-eastward where it influences the hydrography of north Icelandic waters.

20 Volume and heat transport is highly variable and depends strongly on the wind field north of Denmark Strait. Highest monthly mean transport rates at Hornbanki occur in summer (0.75 Sv) when northerly winds are weak, lowest transport is observed in winter (0.35 Sv). Summer heat flux rates (14 TW) can be even three times higher than in winter (4 TW). Strong variability can also be observed on the interannual scale. In 25 particular the winter 2002/2003 showed anomalous high transport and heat flux rates. During the period 1997 to 2003 decreasing northerly winds caused an increase of the NIIC volume and heat transport by 30%, leading to a warming of North Icelandic shelf by around 0.5 K.

OSD

3, 1149–1189, 2006

NIIC modelling

K. Logemann and
I. H. Harms

[Title Page](#)

[Abstract](#)

[Introduction](#)

[Conclusions](#)

[References](#)

[Tables](#)

[Figures](#)

◀

▶

◀

▶

[Back](#)

[Close](#)

[Full Screen / Esc](#)

[Printer-friendly Version](#)

[Interactive Discussion](#)

EGU

1 Introduction

OSD

3, 1149–1189, 2006

The transport of warm and saline Atlantic water masses (AW) northward across the Greenland-Iceland-Scotland ridge is an essential component of the Atlantic Meridional Overturning Circulation (AMOC). Water mass characteristics of the sub-polar North Atlantic, the Arctic ice cover and to a large extent the climate of North-western Europe strongly depend on the intensity of the AMOC. The inflow of AW into the Greenland-Iceland-Norwegian Sea (GIN-sea) occurs via three branches: between Greenland and Iceland through Denmark Strait (1 Sv), between Iceland and the Faroe Islands (3.3 Sv) and through the Faroe-Shetland-Channel (3.7 Sv) (Hansen and Østerhus, 2000).

This study investigates in more detail the transport west of Iceland through Denmark Strait which is the smallest and the most variable flux among all three passages. In the frame of the EU project METACOD¹, a high resolution 3-D hydrodynamic model is set up to trace pathways and fate of cod eggs that are spawned in south Icelandic waters (Brickman et al., 2006²). The egg drift usually follows an anti-cyclonic coastal circulation from the south coast of Iceland, north-westward through Denmark Strait and northward up to the nursery areas along the north coast of Iceland. The drift is part of the North Icelandic Irminger Current (NIIC) that is responsible for the transport of warm and saline Atlantic Waters onto the north Icelandic shelf (Fig. 1). Although this northward transport is small compared to the other through-flows, convection processes in the Iceland Sea and the ecosystem on the north Icelandic Shelf depend on the import of heat, salt and nutrients by the NIIC (Hansen and Østerhus, 2000; Jónsson and Valdimarsson, 2005).

Estimations of the NIIC's volume flux are mostly in the range of 1 Sv (Jónsson and Briem, 2003; Worthington, 1970) but can vary between 0.6 Sv (Stefánsson, 1962) and 2 Sv (Dietrich et al., 1975). Kristmannsson (1989, 1998) emphasizes a strong vari-

¹ METACOD – role of sub-stock structure in the maintenance of cod metapopulations

² Brickman, D., Marteinsdottir, G., Logemann, K., and Harms, I.: Drift Probabilities for Icelandic Cod Larvae, ICES Journal of Marine Science, submitted, 2006.

NIIC modelling

K. Logemann and
I. H. Harms

[Title Page](#)

[Abstract](#)

[Introduction](#)

[Conclusions](#)

[References](#)

[Tables](#)

[Figures](#)

◀

▶

◀

▶

[Back](#)

[Close](#)

[Full Screen / Esc](#)

[Printer-friendly Version](#)

[Interactive Discussion](#)

EGU

ability with transport rates between 0–2.8 Sv. The newest estimation by Jónsson and Valdimarsson (2005) gives 1.1 Sv (66% AW) and latest model results show a NIIC volume transport of 0.5 Sv (Nilsen et al., 2003).

OSD

3, 1149–1189, 2006

2 Model description

5 The 3-dimensional circulation model CODE (Cartesian coordinates Ocean model with three-dimensional adaptive mesh refinement and primitive Equations, Logemann (2006)) was applied. The model uses the primitive equations in a static adaptive finite difference grid, on geopotential vertical levels. The main difference to other adaptive solvers on similar grids, e.g. the model of Khokhlov (1998) or GERRIS (Popinet, 2003),
10 is the avoidance of a (multilevel) Poisson solver when computing the pressure. CODE uses the hydrostatic pressure approximation, i.e. it neglects accelerations caused by vertical pressure gradients which are part of the Poisson equation. The model's treatment of the primitive equations is based on HAMSOM/VOM (Backhaus, 1985) which has been frequently applied to the north-eastern North Atlantic (e.g. Harms et al.,
15 1999a, b, 2000; Logemann et al., 2004). A recent development of HAMSOM/VOM also includes adaptive mesh refinement (Backhaus, 2006³; Harms et al., 2003). However, its refinement is restricted to the vertical and it uses a different organisation of grid cells.

The grid cell organisation in CODE mainly follows the tree algorithm of Khokhlov (1998) that determines the spatial discretisation and grid cell organisation (Fig. 2).
20 The pairs of numbers within the cells (left panel) denote the level of horizontal (first number) and vertical (second number) refinement. A cell with the pair (n, m) has a size of $\Delta x = \Delta x_0 \times 2^{-n}$ in x-direction and $\Delta z = \Delta z_0 \times 2^{-m}$ in z-direction. The level of horizontal refinement n does not vary along the z-axis ensuring well defined water columns for

³Backhaus, J. O.: Adaptation of Vertical Resolution to Topography in the Vector-Ocean-Model (VOM), in preparation, 2006.

NIIC modelling

K. Logemann and
I. H. Harms

[Title Page](#)

[Abstract](#)

[Introduction](#)

[Conclusions](#)

[References](#)

[Tables](#)

[Figures](#)

[◀](#)

[▶](#)

[◀](#)

[▶](#)

[Back](#)

[Close](#)

[Full Screen / Esc](#)

[Printer-friendly Version](#)

[Interactive Discussion](#)

EGU

hydrostatic pressure computation. The large basic cells of the size Δx_0 and Δz_0 , with the pair (0,0) (right panel), are located at the top. Some of these cells were assigned to “children” which are located one row below. These are cells which are refined by one level and which take up the volume of their “parent cell” together. First the refinement is 5 performed horizontally. Only after the maximum horizontal level is reached, the vertical refinement starts. Only the “leaves” (marked red), i.e. the cells without children, are directly used for solving the model equations. The parent cells just obtain the mean properties of their children at each time step.

The sea surface elevation ζ is determined by integrating vertically the equation of 10 continuity. The hydrostatic pressure p at the depth z results from vertical integration of the water's density ρ multiplied with the gravitational acceleration g from the sea surface down to z . Therefore the grid cells have to form well defined water columns 15 (integration paths) and a variation of the horizontal resolution within a water column is omitted. Compared to GERRIS this sets up additional restrictions to the adaptive mesh refinement's spatial structure. On the other hand, the avoidance of solving the Poisson equation saves much computing time. The horizontal pressure gradient (along the x-axis) is computed with

$$\frac{\partial p}{\partial x} = \rho_0 g \frac{\partial \zeta}{\partial x} + g \int_z^{\zeta} \frac{\partial \rho}{\partial x} dz', \quad (1)$$

where $\rho_0 = \text{const.}$ is the fluid's mean density. This way the spurious horizontal pressure 20 gradient caused by computing $\frac{\partial p}{\partial x} = \frac{\partial}{\partial x} \left(\int_z^{\zeta} \rho g dz' \right)$ between two differently resolved water columns are removed. The density gradients are computed with

$$\frac{\partial \rho}{\partial x} = f \left(\frac{\partial T}{\partial x}, \frac{\partial S}{\partial x}, p \right), \quad (2)$$

where f is a linear function of the temperature (T) and salinity (S) gradient, and the

pressure p obtained by a least squares fit to data produced with the UNESCO equation of state (Millero et al., 1980). The remaining spurious horizontal density gradient between two cells of different thickness (caused by spurious temperature and salinity gradients) is avoided by jumping to the next lower level of vertical refinement if necessary (Fig. 3).

Horizontal and vertical turbulence is parameterised by algorithms following Smagorinsky (1963) and Kochergin (Pohlmann, 1996). The Smagorinsky constant is determined through optimisation of model trajectories along the trajectories of (WOCE) surface drifters drogued at 15 m depth (Valdimarsson and Malmberg, 1999). The horizontal diffusion parametrised in this way is equally applied for diffusion of momentum and scalar variables (T , S). Three-dimensional advection of momentum and scalar tracers (T , S) is realized by an FTCS approach (forward in time, centred in space) using the van Leer flux limiter function (van Leer, 1979).

The model domain comprises the North Atlantic and Arctic Ocean (Fig. 4a). The base matrix' resolution is 320 m vertical and between 75 km and 150 km horizontal (higher in polar and sub-polar regions). Close to the sea surface the vertical resolution is increased to 10 m (Fig. 4c). Within the north-east North Atlantic and the Nordic Seas adaptive mesh refinement increases the resolution when approaching Icelandic waters. The maximum resolution is 1.2 km horizontal and 10 m vertical over the entire water column (Figs. 4b and c). The model is eddy resolving over much of Iceland's shelf waters. The topography is based on the IBCAO data set (Jakobsson et al., 2001) for polar and sub-polar regions and on theETOPO-5 data set (Bamber et al., 1997) for the Atlantic/North Atlantic, with a blending technique in the transition zone.

For spin up, CODE was integrated for 10 years on the coarse base grid and for three more years with full resolution. The model is initialised with climatological temperature and salinity data from the PHC world ocean data set (Steele et al., 2001) and forced with ECMWF atmospheric reanalysis data that describes a cyclic stationary, climatological year (Ocean Model Intercomparison Project (OMIP) dataset; Röske, 2001). Ocean temperature and salinity fields were depth independently restored to the

NIIC modelling

K. Logemann and
I. H. Harms

[Title Page](#)

[Abstract](#)

[Introduction](#)

[Conclusions](#)

[References](#)

[Tables](#)

[Figures](#)

[◀](#)

[▶](#)

[◀](#)

[▶](#)

[Back](#)

[Close](#)

[Full Screen / Esc](#)

[Printer-friendly Version](#)

[Interactive Discussion](#)

PHC's monthly fields using a time constant of 30 days. Following the climatological spin up period, the model system is integrated for 8 years (1996–2003), using 6 hourly NCEP/NCAR data for wind stress and direction, air temperature, cloud cover, humidity and precipitation (Kalnay et al., 1996). Runoff data from 11 Icelandic rivers, provided by the Hydrological Service of the Icelandic National Energy Authority, is applied as freshwater volume flux into the model domain (National Energy Authority, 2003). The model results are analysed from 1997 on.

OSD

3, 1149–1189, 2006

NIIC modelling

K. Logemann and
I. H. Harms

3 Model results

3.1 Large scale overview

10 The simulated circulation in the North Atlantic is qualitatively in good agreement with the surface flow deduced from buoy drift, published by Jakobsen et al. (2003). The simulated Irminger Current's structure east and west of the Reykjanes Ridge resembles the circulation schemes given by Dietrich et al. (1975), Bersch (1995) and van Aken and Becker (1996). Also the circulation pattern over the west-Icelandic shelf does not 15 contradict to the observations by Valdimarsson and Malmberg (1999).

Quantitatively, the model slightly underestimates volume fluxes across the Iceland-Scotland ridge (Table 1) compared to observational based values given by Hansen and Østerhus (2000). The simulated amount of inflowing AW through the Greenland-Iceland section is significantly lower than their estimation, which has, on the other hand, 20 an uncertainty of around 1 Sv (Hansen and Østerhus, 2000).

The origin of the NIIC is the cyclonic sub-polar gyre in the Iceland basin with the Irminger Current (IC) as main component (see Fig. 1). In the southwest of the island, the broad flow of the IC breaks into a near shore current that follows the Icelandic coast and an off shore branch that follows the Reykjanes ridge, crosses it further southwest and continues towards Denmark Strait (Fig. 5). Large parts of the IC re-circulate 25 south-west of Denmark Strait and only a small part forms together with the coastal

Title Page	
Abstract	Introduction
Conclusions	References
Tables	Figures
◀	▶
◀	▶
Back	Close
Full Screen / Esc	

Printer-friendly Version
Interactive Discussion

EGU

flow the NIIC. Whereas the off-shore branch is of AW origin ($S > 35.0$) and reaches down to 500 m, the on-shore branch appears as a shallow coastal current that entrains freshwater from land runoff ($S < 35.0$).

The high resolution flow field in Fig. 5 shows a clockwise circulation around Iceland with the warm north-westward flowing branch of the IC as the most prominent feature. The continuation of the IC, the NIIC, flows north-eastward through Denmark Strait and shares the narrow passage with cold, less saline southward flowing polar water masses (PW) of the East Greenland Current (EGC). The collision of warm, saline and cold, fresh water masses results in a distinct front between both systems. The NIIC continues further eastward and reaches the north coast of Iceland where it influences significantly the shelf hydrography. In this area the flow is very much topographically steered. The core of the NIIC lies in approx. 100 m depth just over the 150 m depth contour which is in good agreement with observations (Jónsson and Valdimarsson, 2005). Near surface waters follow closely the shore line along the north coast and flush even smaller fjords up to their inner parts with relative warm and salty AW.

3.2 Spatial variability of the NIIC

In order to assess the spatial variability of the NIIC on its way around Iceland, 15 model sections were defined west and north of the island (Fig. 6). The following analysis is based on the mean climatological flow field from the period 1997–2003.

Table 2 shows, that volume fluxes of the inshore branch (sections 1a, 2a, 3a) are significantly lower than those from the off-shore branch (sections 1b, 2b, 3b). Both branches merge into section 4, that can be regarded as the NIIC origin. A striking feature is that from section 4 on, the transport rates (0.9 Sv) are reduced abruptly by almost 50% down to 0.4 and 0.5 Sv at section 5 and 6, respectively. Further downstream, the volume flux recovers slightly and section 7 yields again a transport of 0.6 Sv. However, despite of this recover, the simulated transport through section 7 remains too low compared to estimations by Jónsson and Valdimarsson (2005) who give 1.1 Sv transport (AW fraction 66%) between 1994 and 2000 through Hornbanki section that is

NIIC modelling

K. Logemann and
I. H. Harms

[Title Page](#)

[Abstract](#)

[Introduction](#)

[Conclusions](#)

[References](#)

[Tables](#)

[Figures](#)

[◀](#)

[▶](#)

[◀](#)

[▶](#)

[Back](#)

[Close](#)

[Full Screen / Esc](#)

[Printer-friendly Version](#)

[Interactive Discussion](#)

EGU

equivalent to our section 7.

The spatial variability of the volume flux is also reflected in the heat flux rates (relative to 0°C), presented in the last row in Table 2. The contribution of the in-shore pathway to the total heat flux through section 4 (18 TW) is approx. 15–20%. The major part of the
5 heat advection by the NIIC is thus made up by AW from the sub-polar gyre (sections 1b, 2b and 3b). Like with the volume flux, the heat transport breaks down after section 4 but recovers and stabilizes on the following sections downstream. The mean temperature, however, drops more or less continuously whereas the mean salinity remains stable from section 6 on and even increases slightly towards the last two sections.

10 3.3 Temporal variability of the NIIC

3.3.1 High frequent variability (days – months)

Near-shore or shelf transport rates (sections 1a, 2a and 3a) are highly variable in time. Daily mean values and corresponding standard deviations for at these sections are similar in magnitude (0.25 Sv, 0.16 Sv and 0.17 Sv, respectively) and maximum
15 transport rates of 1 Sv may occur in both directions. Strong variability is also observed further upstream at section 7, where extreme values for the volume flux range from e.g. 0.84 Sv (31 January 2002) to –1.91 Sv (3 February 2002) (Fig. 7). The standard deviation for daily mean volume fluxes is 0.32 Sv. Similar variability can be observed for the temperature and salinity distribution. At section 7, the model gives a standard deviation of 0.29 K and 0.034 psu.

20 The mean heat flux through section 7 is 9 TW with a standard deviation of 0.5 TW. Comparing the contributions of volume flux (M) and temperature (T) to the heat flux variability by comparing the sums

$$\sum_{\text{day}} |M_{\text{day}} - \bar{M}| \bar{T} \rho c_p$$

NIIC modelling

K. Logemann and
I. H. Harms

[Title Page](#)

[Abstract](#)

[Introduction](#)

[Conclusions](#)

[References](#)

[Tables](#)

[Figures](#)

[◀](#)

[▶](#)

[◀](#)

[▶](#)

[Back](#)

[Close](#)

[Full Screen / Esc](#)

[Printer-friendly Version](#)

[Interactive Discussion](#)

and

$$\sum_{\text{day}} |T_{\text{day}} - \bar{T}| \bar{M} \rho c_p$$

we can conclude that the volume flux is responsible for 68% of the heat flux variability and only 32% is due to variability of the mean temperature on section 7 (seasonal signal included).
5

3.3.2 Seasonal variability

The analysis of the yearly cycle of NIIC transport rates and heat fluxes on section 7 together with mean temperatures on the north-Icelandic shelf, averaged for 1997–2003, shows a very pronounced seasonal signal (Fig. 8). All three variables show maximum 10 values in spring/summer and minimum values in autumn/winter. The largest amplitude is visible for the heat flux curve where the summer value is more than three times higher than the winter value. This seasonal switch is due to the fact that the temperature evolution and volume flux are in phase, however with a time lag of 4 months.

An explanation for the strong seasonal variability of the NIIC can be found in the 15 wind forcing. The dependency of transport rates on local wind stress is apparent in a comparison of time series of the NCEP northerly wind component and the simulated northward NIIC transport. Both curves show an almost identical behaviour (Fig. 9) which indicates that negative (northerly) wind stress reduces or even blocks the NIIC. The rather abrupt reduction in northerly wind stress in March/May down to the lower 20 summer level is followed by a continuous increase from September to February. The NIIC responds directly to that wind signal and shows higher transport rates in particular during the summer months.

There is a distinct trend visible in Fig. 9 for the north component of the wind stress and also for the volume flux. During the period 1997 to 2003 decreasing northerly 25 winds caused an increase of the NIIC volume flux by 30% which results in a similar heat flux increase. The analysis of spatially averaged temperatures shows that from

NIIC modelling

K. Logemann and
I. H. Harms

[Title Page](#)

[Abstract](#)

[Introduction](#)

[Conclusions](#)

[References](#)

[Tables](#)

[Figures](#)

[◀](#)

[▶](#)

[◀](#)

[▶](#)

[Back](#)

[Close](#)

[Full Screen / Esc](#)

[Printer-friendly Version](#)

[Interactive Discussion](#)

1997–2003, the positive heat flux trend leads to a warming of the North Icelandic shelf by 0.49 K.

3.3.3 Interannual variability

Although the relative strong temperature and salinity restoring (c.f. Sect. 2) damps variability on longer time scales, the model shows distinct interannual signals. A time series of NIIC transport anomalies together with temperature and heat flux anomalies (Fig. 10) reveals anomalous high volume fluxes during winter 1997/1998, 2000/2001 and 2003/2004. These periods are also characterized by enhanced northward heat flux and positive temperature anomalies on the north Icelandic shelf. A particular extreme situation occurred in winter 2003/2004 when all three curves showed very distinct positive anomalies. The anomalous warming, which is also apparent in observed horizontal temperature distributions (<http://www.hafro.is/Sjora>), is caused primarily by an unusual wind event that lasted for the whole winter season 2003/2004: Instead of being blocked by strong northerly wind stress, as usual during winter, the NIIC remained on a rather high level because of weak or missing northerly winds. This anomalous wind situation leads to an additional effect that even enhanced the 2003/2004 event: Cooling and convection south-west of Iceland were weakened during winter 2003/2004 due to missing advection of cold air masses from the north. As a result, the surface waters in the NIIC source region remain much warmer than in previous years (Fig. 11). The 2003/2004 anomaly is thus a combined effect of i) enhanced northward advection of ii) unusual warm waters towards the north Icelandic shelf.

Although there seems to be a strong link between heat flux and mean temperature on the north Icelandic shelf, negative volume flux anomalies like during winter 1998/1999 do not necessarily cause negative temperature anomalies north of Iceland. Whereas volume and heat flux are obviously well correlated, the comparison between heat flux and temperature anomaly gives a correlation of only 0.75, based on a time lag of 17 days. This means that roughly 57% of the temperature evolution on the north Icelandic shelf can be explained by heat advection through the NIIC. The remaining 43% are

NIIC modelling

K. Logemann and
I. H. Harms

[Title Page](#)

[Abstract](#)

[Introduction](#)

[Conclusions](#)

[References](#)

[Tables](#)

[Figures](#)

[◀](#)

[▶](#)

[◀](#)

[▶](#)

[Back](#)

[Close](#)

[Full Screen / Esc](#)

[Printer-friendly Version](#)

[Interactive Discussion](#)

determined by other process such as the entrainment rate of PW from the north or local atmospheric heat exchange.

3.4 Origins, pathways and composition of NIIC waters: a tracer study

The analysis of simulated climatological flow fields suggest, that the NIIC is composed of an in-shore branch crossing the south Icelandic shelf and an off-shore branch in deep waters, mainly fed by AW from the IC. Both sources merge into Denmark Strait where the NIIC collides with the EGC, that flows in opposite direction. In the frontal zone, some parts of the NIIC re-circulate, other parts continue northward, mixing with PW on its way north-westward. In order to define the upstream pathways and origins of the NIIC and to determine the extent of mixing, a tracer dispersion model based on climatological flow fields (1997–2003) is applied.

The focus is on model section 7 (Hornbanki), where a volume of $2.5 \times 10^{11} \text{ m}^3$ of NIIC-water is marked with passive tracers. These tracers are advected backward in time and the tracer flux through different sections is integrated over three years. The model results are depicted in Fig. 12. Vectors show the vertically integrated tracer flux over 3 years, originating from the marked volume in section 7 (i.e. the white line denoting 100%), following the integral

$$\int_{t=0}^{t=3} \int_{z=-D}^{z=\zeta} c \mathbf{v} dz dt$$

where c denotes the dimensionless tracer concentration and \mathbf{v} the current vector. The vectors have the unit (m^2). At the white sections, the percentage of the initial volume is given, which has passed these lines during three years of calculation.

The dispersion model shows a surprisingly high amount of PW (57%) that is entrained into the NIIC. Only 43% originates from south of Denmark Strait, consisting of approx. 29% sub-polar gyre AW (i.e. the off-shore branch) and 14% waters from the south Icelandic shelf (i.e. the in-shore branch).

NIIC modelling

K. Logemann and
I. H. Harms

[Title Page](#)

[Abstract](#)

[Introduction](#)

[Conclusions](#)

[References](#)

[Tables](#)

[Figures](#)

[◀](#)

[▶](#)

[◀](#)

[▶](#)

[Back](#)

[Close](#)

[Full Screen / Esc](#)

[Printer-friendly Version](#)

[Interactive Discussion](#)

Vertical profiles along the source pathways of the NIIC (Fig. 13) show that the entrained PW originates from the upper 200 m of the EGC (profile 13a) whereas the AW from south of Denmark Strait is more evenly distributed over the whole depth range between 0–1000 m (profile 13g and h). The in-shore branch (profile 13d) contributes to the NIIC with high concentrations at the surface whereas the off-shore branch (profile 13c) reveals a bi-modal structure with high concentrations at the surface and in 150 m depth. The core of the NIIC close to section 7 is located in 100 m depth (profile 13b).

A remarkable feature is the vertical structure at the far upstream profile 13h, where tracers are concentrated in depths between 400 and 600 m. The source for water masses at that position and in those depths is most likely the overflow coming across the Iceland-Faeroe ridge or through the Faeroe-Scotland channel. Compared to profile 13e, g and h, profile 13f shows the shallowest core location south of Iceland, in less than 100 m depth. The reason for this subsurface maximum is frequently observed upwelling at the continental slope along the south coast.

Based on time series of the NIIC throughflow from 1997–2003 (c.f. Sect. 3.3.2), we determined two periods, one with maximum transport rates (8 September 2002–9 September 2003, NIIC at section 7=0.7 Sv) and one with minimum transport rates (15 October 1998 – 14 October 1999, NIIC at section 7=0.5 Sv). Extracted flow fields were used to repeat the tracer experiment for these two periods. The model results confirmed, that with increasing NIIC volume transport the fraction of AW rises simultaneously (Fig. 14), during the 2002/2003 period up to 46%. However, the intensification of AW inflow in 2002/2003 is mainly through the off-shore branch. The in-shore branch even decreases in that period from 10% (1998/1999) down to 8%.

4 Discussion

The spatial variability of the NIIC is characterized by a break down and recover of simulated volume and heat transport along the west coast of Iceland. Two reasons are responsible for that feature: a) the re-circulation of AW in Denmark Strait and b) the

NIIC modelling

K. Logemann and
I. H. Harms

[Title Page](#)

[Abstract](#)

[Introduction](#)

[Conclusions](#)

[References](#)

[Tables](#)

[Figures](#)

◀

▶

◀

▶

[Back](#)

[Close](#)

[Full Screen / Esc](#)

[Printer-friendly Version](#)

[Interactive Discussion](#)

EGU

entrainment of PW along the fronts in Denmark Strait and further downstream, in the north-western waters. Based on the simulated climatological volume and heat fluxes and on the dispersion patterns of the tracer study in 3.4, Fig. 15 presents a schematic sketch of NIIC pathways and transport rates.

5 The separation of the NIIC from the IC occurs mainly between section 3 and 4. Approximately 90% of the AW re-circulate here and only 10% of the IC contribute to the NIIC. If we assume that the inshore branch feeds completely into the NIIC, we can state that this pathway contributes approx. 20% (0.2 Sv) whereas the off-shore branch contributes 80% (0.7 Sv) to the total volume flux through section 4 (0.9 Sv).

10 A further reduction of the NIIC due to re-circulating AW occurs between section 4 and 5, where in particular the volume flux drops from 0.9 to 0.4 Sv. But also the heat flux is reduced from 18 TW down to 7 TW, the mean salinity falls from 34.88 down to 34.72 and the mean temperature drops by half a degree (c.f. Table 2). The reduction in volume and heat transport suggests a further re-circulation of AW in the range of 15 0.6 Sv whereas the drop in mean salinity can only be explained by entrainment of PW which should be in a range of 0.1 Sv.

On the following sections 6 and 7, transport and heat flux remain stable (it even recover slightly) but the mean temperature and salinity continues to fall. To meet these constraints, further entrainment of PW is needed. The total transport through section 20 7 (0.6 Sv) is finally made up of roughly 0.3 Sv PW and 0.3 Sv AW which would be consistent with the results of the tracer study (47% AW versus 53% PW).

Although this sketch gives a rather comprehensive view of the NIIC pathway, we clearly see discrepancies between model results and observations. In contrast to our model findings, Jónsson and Valdimarsson (2005) estimate from observations that 25 66% AW (south of Denmark Strait) and only 34% PW (north of Denmark Strait) contributes to the Hornbanki throughflow (i.e. section 7). There are also indications that simulated mean salinity and temperatures are too low and too fresh compared to observations. We therefore argue that the simulated low AW amount and the strong entrainment of PW in the model leads to a rapid fading of the NIIC signal that is con-

NIIC modelling

K. Logemann and
I. H. Harms

[Title Page](#)

[Abstract](#)

[Introduction](#)

[Conclusions](#)

[References](#)

[Tables](#)

[Figures](#)

[◀](#)

[▶](#)

[◀](#)

[▶](#)

[Back](#)

[Close](#)

[Full Screen / Esc](#)

[Printer-friendly Version](#)

[Interactive Discussion](#)

EGU

5 nected with too low salinity, temperature and heat flux rates. This also explains why the values of modelled and observed inflowing AW given in Table 1 disagree for the Greenland – Iceland passage. A further indication for an overestimated fading of the simulated NIIC signal is the fact that model section 4 (0.9 Sv AW, 18 TW) agrees well with the Hornbanki observations at section 7 (0.75 Sv AW, 18.9 TW) although model section 4 is much more upstream than Hornbanki.

10 Reasons for an overestimated weakening of the NIIC signal can be manifold. It can be speculated that even the high resolution of less than 5 km on the Icelandic shelf is still too coarse to capture the entrainment processes along the fronts between AW and PW. The atmospheric forcing could also play a role: currently NCEP data is used which has a spatial resolution of roughly 2° (230 km). Denmark Strait is covered by one or two grid points which does not allow any spatial variability in wind forcing to occur. The third candidate for too strong fading of the NIIC could be the parameterised horizontal diffusion. Turbulent exchange coefficients might be still too high, although 15 these parameters were optimised in a validation exercise that compared intensively model trajectories in this area with observed buoy drifts (Valdimarsson and Malmberg, 1999).

20 The underestimation of NIIC inflow of AW is a common problem in many model studies (e.g. Karcher et al., 2003; Nilsen et al., 2003; Drange et al., 2005; Griffies et al., 2005; Oka and Hasumi, 2006) mainly because of too coarse resolution in model grid and forcing data. Although there are still some discrepancies, the present application is the highest resolving model of that area which is able to reproduce a fairly well established NIIC. This allows a closer look especially on driving mechanisms of the NIIC.

25 A vertical section north of Denmark Strait shows, that just above the shelf break of west Iceland, the southward flowing branch of the EGC forms a distinct front to the northward flowing NIIC (Fig. 16). The NIIC is pushed onto the Icelandic shelf which means that deeper parts of the AW inflow are cut off and have to re-circulate southward without entering Denmark Strait. If the southward flowing EGC branch gets

NIIC modelling

K. Logemann and
I. H. Harms

[Title Page](#)

[Abstract](#)

[Introduction](#)

[Conclusions](#)

[References](#)

[Tables](#)

[Figures](#)

[◀](#)

[▶](#)

[◀](#)

[▶](#)

[Back](#)

[Close](#)

[Full Screen / Esc](#)

[Printer-friendly Version](#)

[Interactive Discussion](#)

even stronger and broadens, the Denmark Strait throughflow of AW could be totally blocked or suppressed. The northward flowing NIIC would then be mainly controlled by the strength of the southward flowing EGC, which suggests a kind of hydraulic control.

Further model investigations revealed that the main forcing for this control mechanism is the time dependant, local wind field. The comparison between NIIC transport rates and daily mean wind fields shows a maximum correlation of 0.86 between the north component of the wind-stress at 67°40' N, 22°32' W and the volume flux through section 7 (Fig. 17). This rather good correlation indicates that the NIIC transport is significantly reduced if northerly winds enforce the EGC. The cross spectral analysis of both time series reveals, that this mechanism mainly explains the seasonal and interannual variability. Obviously the NIIC does not respond to the synoptic atmospheric scale in the range of a few days. Only for periods larger than three days the correlation increases up to a distinct maximum at 24 and 29 days. The total maximum at 365 days reflects the seasonal signal.

However, two points have to be mentioned in this context: a) the spatial resolution of the NCEP forcing data is, as already mentioned, rather coarse and b) the analysis of volume flux versus wind stress is based on daily mean values. High frequent and small scale features like e.g. fast moving polar lows are thus insufficiently resolved. The synoptic scale between one and three days (i.e. the storm frequency) might therefore be underestimated in the spectral analysis.

The dispersion model results concerning origin, pathways and composition of NIIC tracers have important implications for the assessment of cod egg drift, the main motivation for this model study. Since the south Icelandic shelf is the main spawning area for cod, the drift of spawned eggs depend mostly on the intensity of the in-shore coastal flow which has only a small share in the NIIC composition. Even more important in this respect is the fact that the in-shore branch shows a different behaviour than the IC and NIIC signals: during years with high NIIC transport rates, the tracer contribution from the off-shore IC increased equivalently whereas the in-shore contribution even decreased. This means that the NIIC transport observed at Hornbanki does not nec-

NIIC modellingK. Logemann and
I. H. Harms[Title Page](#)[Abstract](#)[Introduction](#)[Conclusions](#)[References](#)[Tables](#)[Figures](#)[|◀](#)[▶|](#)[◀](#)[▶](#)[Back](#)[Close](#)[Full Screen / Esc](#)[Printer-friendly Version](#)[Interactive Discussion](#)

essarily reflect the intensity of cod egg drift around Iceland and hence the strength of year classes appearing in the north.

OSD

3, 1149–1189, 2006

5 Conclusions

The ocean model CODE produces circulation patterns which are in good agreement with the general view of the currents around Iceland. Based on detailed analysis of fluxes of volume, heat and passive tracers, the paper presents a comprehensive view of the origins, pathways and composition of NIIC water masses. Concerning the ratio of AW and PW in the NIIC, the model shows some discrepancies with observations. Whereas the model suggests an almost equivalent AW/PW ratio (0.43/0.57), Jónsson and Valdimarsson (2005) give a AW/PW ratio of approx. 0.7/0.3. A comparison of simulated volume fluxes, mean temperature and salinity with observational data from various sections within the NIIC indicate that the entrainment of PW could be overestimated in the model. Possible reasons are too coarse grid resolution in AW/PW frontal zones, too coarse atmospheric forcing data that suppresses spatial variability or too strong horizontal mixing.

Despite obvious differences in the composition of the NIIC, the model allows to determine the origin of NIIC water masses coming from the south (i.e. the AW composition). Two sources could be found: the Irminger Current flowing off-shore in deep water along the Reykjanes Ridge and the in-shore coastal component, flowing on the south Icelandic shelf. The main source for AW in the NIIC (at *Hornbanki*) is the off-shore Irminger Current as part of the sub-polar gyre (66%). South Icelandic shelf waters contribute only 33% to the NIIC which implies that the Irminger Current has a two times stronger influence on the NIIC water mass composition than the coastal component. Given the AW/PW ratio of Jónsson and Valdimarsson (2005) and our ratio for the AW composition we can estimate the fractions of the NIIC components as follows: 33% PW from the EGC, 44% AW from the IC and 22% south Icelandic shelf water.

The seasonal variability of the NIIC is considerable and mainly influenced by local

NIIC modelling

K. Logemann and
I. H. Harms

[Title Page](#)

[Abstract](#)

[Introduction](#)

[Conclusions](#)

[References](#)

[Tables](#)

[Figures](#)

[◀](#)

[▶](#)

[◀](#)

[▶](#)

[Back](#)

[Close](#)

[Full Screen / Esc](#)

[Printer-friendly Version](#)

[Interactive Discussion](#)

EGU

northerly wind stress. Highest transport rates occur in summer when northerly winds are weak. The increase of volume transport falls together with the surface temperature increase due to atmospheric and solar warming. Both processes lead to a more than three times higher heat flux rate in summer than in winter. Strong variability can also be observed on the interannual scale. In particular the winter 2002/2003 showed unusual high transport and heat flux rates that are responsible for the observed temperature anomaly in North Icelandic waters during that time. The model indicates furthermore a clear trend for the period 1997–2003: due to weaker northerly winds, northward transport of the NIIC increased by roughly 30% which caused a warming of the North Icelandic shelf by roughly 0.5 K during that period. Further modelling has to clarify whether this is a long term trend that continues after 2003.

The drift of cod eggs, which is the main motivation for this model study, depends very much on the in-shore flow across south-west Icelandic waters since the major spawning areas are located here (Storr-Paulsen et al., 2004; Brickman et al., 2006²). The model indicates so far that the in-shore branch is to a certain extent uncoupled from the large scale IC which presents the major source for the NIIC. Linking the intensity of cod egg drift or even the strength of year classes to NIIC or IC indices might thus be very critical and lead to wrong assumptions. Future modelling of egg drift around Iceland has to resolve sufficiently good the time and space variability of the coastal flow on the shelf which requires eddy resolving models forced with high resolution atmospheric data. The present model is eddy resolving on most of the Icelandic shelf but the general lack of high quality forcing data inhibits so far a more detailed study of the coastal flow. Further investigation and model improvement is needed in this field.

NIIC modelling

K. Logemann and
I. H. Harms

[Title Page](#)

[Abstract](#)

[Introduction](#)

[Conclusions](#)

[References](#)

[Tables](#)

[Figures](#)

[|◀](#)

[▶|](#)

[◀](#)

[▶](#)

[Back](#)

[Close](#)

[Full Screen / Esc](#)

[Printer-friendly Version](#)

[Interactive Discussion](#)

EGU

Acknowledgements. The model development and analyses have been supported by the EU-project METACOD (Q5RS-2001-00953). The authors would like to thank H. Valdimarsson for providing surface drifter data. Thanks to J. Mortensen and D. Quadfasel for helpful comments.

OSD

3, 1149–1189, 2006

References

5 Backhaus, J. O.: A three-dimensional model for the simulation of shelf sea dynamics, Deutsche hydrographische Zeitschrift, 38, 165–187, 1985.

Bamber, J., Muller, J. P., and Mandanayake, A.: A Global 5 Arc Minute Digital Elevation Model Derived from the Geodetic Phase of ERS-1. Proc. 3rd ERS Symp. On space of the service of our environment, Florenz, 1997.

10 Bersch, M.: On the circulation of the north-eastern North Atlantic, Deep Sea Res., 42, 1583–1607, 1995.

Dietrich, G., Kalle, K., Krauss, W., and Siedler, G.: General Oceanography, 2nd ed., John Wiley and Sons, New York, 626 pp., 1975.

15 Drange, H., Gerdes, R., Gao, Y., Karcher, M., Kauker, F., and Bentsen, M.: Ocean General Circulation Modelling of the Nordic Seas, in: The Nordic Seas: An Integrated Perspective, edited by: Drange, H., Dokken, T., Furevik, T., Gerdes, R., and Berger, W., AGU Monograph 158, AGU, Washington DC, 199–220, 2005.

20 Griffies, S. M., Gnanadesikan, A., Dixon, K. W., Dunne, J. P., Gerdes, R., Harrison, M. J., Rosati, A., Russell, J. L., Samuels, B. L., Spelman, M. J., Winton, M., and Zhang, R.: Formulation of an ocean model for global climate simulations, Ocean Sci., 1, 45–79, 2005.

25 Hansen, B. and Østerhus, S.: North Atlantic-Nordic Seas exchanges, Progress in Oceanography, 45, 109–208, 2000.

Harms, I. H., Backhaus, J. O., and Hainbucher, D.: Modelling the seasonal variability of circulation and hydrography in the Iceland-Faeroe-Shetland overflow area, ICES CM 1999/L:10, Annual Science Conference, 29 September to 2 October 1999, Stockholm, Sweden, 1999a.

25 Harms, I. H., Backhaus, J. O., and Hainbucher, D.: The circulation in the EU-TASC-region during the Calanus year 1996/1997 ICES CM 1999/L:33, Annual Science Conference, 29 September to 2 October 1999, Stockholm, Sweden, 1999b.

30 Harms, I. H., Heath, M., Bryant, A., Backhaus, J. O., and Hainbucher, D.: Modeling the north-east Atlantic circulation - Implications for the spring invasion of shelf regions by Calanus

NIIC modelling

K. Logemann and
I. H. Harms

[Title Page](#)

[Abstract](#)

[Introduction](#)

[Conclusions](#)

[References](#)

[Tables](#)

[Figures](#)

[◀](#)

[▶](#)

[◀](#)

[▶](#)

[Back](#)

[Close](#)

[Full Screen / Esc](#)

[Printer-friendly Version](#)

[Interactive Discussion](#)

EGU

5 Harms, I. H., Hübner, U., Backhaus, J. O., Kulakov, M., Stanovoy, V., Stepanets, O., Kodina, L., and Schlitzer, R.: Salt intrusions in Siberian river estuaries: Observations and model experiments in Ob and Yensie, in: Siberian river runoff in the Kara Sea: Characterisation, quantification, variability and environmental significance, edited by: Stein R., Fahl, K., Fütterer, D. F., Galimov, F. M., and Stepanets, O. V., Proceedings in Marine Science, Vol. 6, Elsevier Amsterdam 2003, ISBN 0-444-51365-5, 484 pp., 2003.

10 Jakobsson P. K. and IBCAO Editorial Board Members: Improvement to the International Bathymetric Chart of the Arctic Ocean (IBCAO): Updating the Data Base and the Grid Model. *Eos, Transactions, American Geophysical Union*, 84, 2001.

15 Jakobsen, P. K., Rønnegaard, M. H., Quadfasel, D., Schmitt, T., and Hughes, C. W.: Near-surface circulation in the northern North Atlantic as inferred from Lagrangian drifters: Variability from the mesoscale to the interannual, 2003.

19 Jónsson, S. and Briem, J.: Flow of Atlantic Water west of Iceland and onto the north Icelandic Shelf, ICES Marine Science Symposia, 219, 326–328, 2003.

20 Jónsson, S. and Valdimarsson, H.: The flow of Atlantic water to the North Icelandic Shelf and its relation to the drift of cod larvae, ICES Journal of Marine Science, 62, 1350–1359, 2005.

25 Kalnay, E., Kanamitsu, M., Kistler, R., Collins, W., Deaven, D., Gandin, L., Iredell, M., Saha, S., White, G., Woollen, J., Zhu, J., Chelliah, M., Ebisuzaki, W., Higgins, W., Janowiak, K., Mo, K., Ropelewski, C., Wang, J., Leetmaa, A., Reynolds, R., Jenne, R., and Joseph, D.: The NCEP/NCAR 40-year reanalysis project, *Bull. Am. Meteorol. Soc.*, 77, 437–471, 1996.

29 Karcher, M. J., Gerdes, R., Kauker, F., and Köberle, C.: Arctic warming: Evolution and spreading of the 1990s warm event in the Nordic Seas and the Arctic Ocean, *J. Geophys. Res.*, 108, 3034, doi:10.1029/2001JC001265, 2001.

30 Khokhlov, A. M.: Fully threaded tree algorithms for adaptive refinement fluid dynamics simulations, *J. Comp. Phys.* 143, 2, 519–543, 1998.

Kristmannsson, S. S., Malmberg, S. A., and Briem, J.: Inflow of warm Atlantic water to the subarctic Iceland Sea, *Rapports et Procès-Verbaux des Réunions du Conseil International pour l'Exploration de la Mer*, 188, 74, 1989.

Kristmannsson, S. S.: Flow of Atlantic Water into the northern Icelandic shelf area, 1985–1989, ICES Cooperative Research Report, 225, 124–135, 1998.

IIIC modelling

K. Logemann and
I. H. Harms

[Title Page](#)

[Abstract](#)

[Introduction](#)

[Conclusions](#)

[References](#)

[Tables](#)

[Figures](#)

◀

▶

◀

▶

[Back](#)

[Close](#)

[Full Screen / Esc](#)

[Printer-friendly Version](#)

[Interactive Discussion](#)

EGU

Logemann, K., Backhaus, J. O., and Harms, I. H.: SNAC: a statistical emulator of the north-east Atlantic circulation Ocean Modelling, 7, 97–110, 2004.

Logemann, K.: Modelluntersuchung zur Erwärmung des Bodenwassers der Grönlandsee, Ph.D. thesis, University of Hamburg, 160 pp., 2006.

5 Millero, F. J., Chen, C.-T., Bradshaw, A., and Schleicher, K.: A New High Pressure Equation of State for Seawater. *Deep Sea Res.*, 27, 255–264, 1980.

National Energy Authority, Hydrological Service: Hydrological Service Database, service nr. 10 2003/33, Reykjavik, Iceland, 2003.

Nilsen, J. E.Ø., Gao, Y., Drange, H., Furevik, T., and Bentsen, M.: Simulated North Atlantic- 10 Nordic Seas water mass exchange in an isopycnic coordinate OGCM, *Geophys. Res. Lett.*, 30, 1536, doi:10.1029/2002GL016597, 2003.

Oka, A. and Hasumi, H.: Effects of model resolution on salt transport through northern high- 15 latitude passages and Atlantic meridional overturning circulation, *Ocean Modelling*, in press, doi:10.1016/j.ocemod.2005.12.004, 2006.

Pohlmann, T.: Calculating the annual cycle of the vertical eddy viscosity in the North Sea with a three-dimensional baroclinic circulation model, *Continental Shelf Res.*, 16, 147–161, 1996.

Popinet, S.: Gerris: a tree-based adaptive solver for the incompressible Euler equations in complex geometries, *J. Comp. Phys.*, 190, 572–600, 2003.

Röske, F.: An atlas of surface fluxes based on the ECMWF-Reanalysis – A climatological data 20 set to force global ocean general circulation models, MPI Report, 323, Max-Planck-Inst. f. Meteorologie, Hamburg, pp. 31, 2001.

Smagorinsky, J.: General Circulation Experiments with the Primitive Equations, I. The Basic Experiment, *Mon. Wea. Rev.*, 91, 99–106, 1963.

Steele, M., Morley, R., and Ermold, W.: PHC: A global ocean hydrography with a high quality 25 Arctic Ocean, *J. Climate*, 14, 2079–2087, 2001.

Stefánsson, U.: North Icelandic Waters. *Rit Fiskideildar*, 3, 269 pp., 1962.

Storr-Paulsen, M., Harms, I., Logemann, K., Wieland, K., and Rätz, H.-J.: The impact of 30 environmental conditions on distribution, transport and migration for cod (*Gadus morhua*) in East and West Greenland waters ICES Symposium on “The Influence of Climate Change on North Atlantic Fish stocks”, Bergen, Norway, 2004.

Valdimarsson, H. and Malmberg, S. A.: Near-surface circulation in Icelandic waters derived from satellite tracked drifters, *Rit Fiskideildar*, 16, 23–39, 1999.

van Aken, H. M. and Becker, G.: Hydrography and through-flow in the north-eastern North

NIIC modelling

K. Logemann and
I. H. Harms[Title Page](#)[Abstract](#)[Introduction](#)[Conclusions](#)[References](#)[Tables](#)[Figures](#)[◀](#)[▶](#)[◀](#)[▶](#)[Back](#)[Close](#)[Full Screen / Esc](#)[Printer-friendly Version](#)[Interactive Discussion](#)

EGU

5

Atlantic Ocean: the Nansen project, *Progress in Oceanography*, 38, 297–346, 1996.
van Leer, B.: Towards the Ultimate Conservative Difference Scheme, V: A Second Order Sequel
to Godunov's Method, *J. Comput. Phys.*, 32, 101–136, 1979.
Worthington, L. V.: The Norwegian Sea as a Mediterranean Basin, *Deep-Sea Res.*, 17, 77–84,
1970.

OSD

3, 1149–1189, 2006

NIIC modelling

K. Logemann and
I. H. Harms

[Title Page](#)

[Abstract](#)

[Introduction](#)

[Conclusions](#)

[References](#)

[Tables](#)

[Figures](#)

◀

▶

◀

▶

[Back](#)

[Close](#)

[Full Screen / Esc](#)

[Printer-friendly Version](#)

[Interactive Discussion](#)

EGU

NIIC modelling

K. Logemann and
I. H. Harms

Table 1. Comparison between simulated and observed volume fluxes in the overflow region.

overflow section	model	Hansen and Østerhus (2000)
Iceland-Scotland northward inflow of AW (Sv)	6.7	7
Iceland-Scotland overflow (Sv)	2.9	3
Greenland-Iceland northward inflow of AW (Sv)	0.3	1
Greenland-Iceland overflow (Sv)	2.4	3

[Title Page](#)[Abstract](#)[Introduction](#)[Conclusions](#)[References](#)[Tables](#)[Figures](#)[|◀](#)[▶|](#)[◀](#)[▶](#)[Back](#)[Close](#)[Full Screen / Esc](#)[Printer-friendly Version](#)[Interactive Discussion](#)

EGU

Table 2. Simulated volume flux, mean temperature, salinity and heat flux (relative to 0°C) averaged over the years 1997–2003 at 15 model sections (see Fig. 6).

section	volume flux (Sv)	T (°C)	S (psu)	heat flux (TW)
1a	0.1	7.41	34.93	3
2a	0.2	6.96	35.00	5
3a	0.2	5.87	34.90	5
1b	12	6.21	35.06	300
2b	11	6.03	35.05	270
3b	8	5.78	35.03	190
4	0.9	5.04	34.88	18
5	0.4	4.50	34.72	7
6	0.5	3.63	34.60	8
7	0.6	3.43	34.61	9
8	0.6	3.54	34.48	9
9	0.7	3.37	34.63	10
10	0.5	3.38	34.66	8
11	0.7	2.51	34.72	8
12	0.9	1.68	34.71	8

NIIC modelling

K. Logemann and
I. H. Harms

[Title Page](#)

[Abstract](#) [Introduction](#)

[Conclusions](#) [References](#)

[Tables](#) [Figures](#)

◀

▶

◀

▶

Back

Close

[Full Screen / Esc](#)

[Printer-friendly Version](#)

[Interactive Discussion](#)

EGU

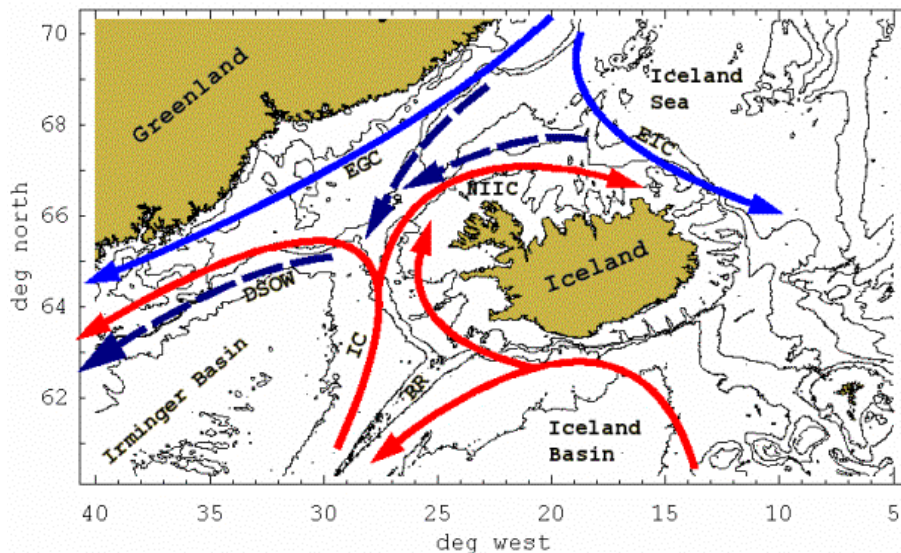


Fig. 1. Bathymetry around Iceland in depth intervals of 200, 500, 1000, 2000 and 3000 m. Red arrows: Atlantic Water (AW), blue arrows: Polar and Arctic Waters (PW) and dashed blue arrows: Denmark Strait Overflow Water (DSOW). Other abbreviations are: EGC – East Greenland Current, EIC – East Icelandic Current, IC – Irminger Current, NIIC – North Icelandic Irminger Current, RR – Reykjanes Ridge.

NIIC modelling

K. Logemann and
I. H. Harms

[Title Page](#)

[Abstract](#)

[Introduction](#)

[Conclusions](#)

[References](#)

[Tables](#)

[Figures](#)

◀

▶

◀

▶

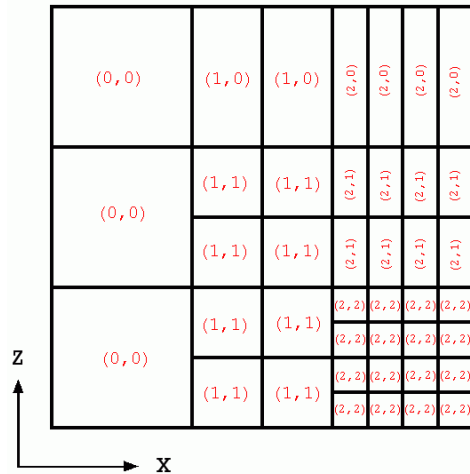
[Back](#)

[Close](#)

[Full Screen / Esc](#)

[Printer-friendly Version](#)

[Interactive Discussion](#)



(hor. level, ver. level)

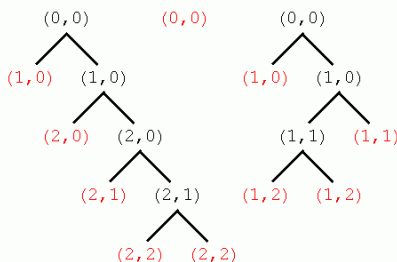


Fig. 2. Scheme of the computational mesh consisting of differently sized cells (left) and scheme of the mesh producing tree algorithm (right).

NIIC modelling

K. Logemann and
I. H. Harms

[Title Page](#)

[Abstract](#)

[Introduction](#)

[Conclusions](#)

[References](#)

[Tables](#)

[Figures](#)

[|◀](#)

[▶|](#)

[◀](#)

[▶](#)

[Back](#)

[Close](#)

[Full Screen / Esc](#)

[Printer-friendly Version](#)

[Interactive Discussion](#)

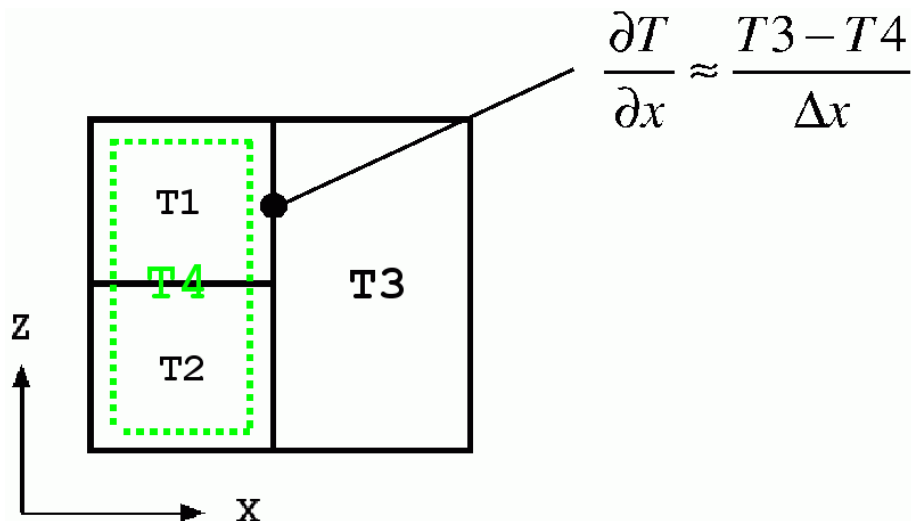


Fig. 3. The computational scheme for the horizontal gradient of temperature or salinity between grid cells of different thickness. Consider the horizontal homogenous but stratified case. I.e. $0.5 \times (T1 + T2) = T3$ and $T1 \neq T2$. In order to avoid the spurious gradient between T1 and T3 the gradient is computed between T3 and the parent cell of T1, the cell T4 = $0.5 \times (T1 + T2)$. Hence the horizontal gradient is zero.

NIIC modelling

K. Logemann and
I. H. Harms

[Title Page](#)

[Abstract](#)

[Introduction](#)

[Conclusions](#)

[References](#)

[Tables](#)

[Figures](#)

[◀](#)

[▶](#)

[◀](#)

[▶](#)

[Back](#)

[Close](#)

[Full Screen / Esc](#)

[Printer-friendly Version](#)

[Interactive Discussion](#)

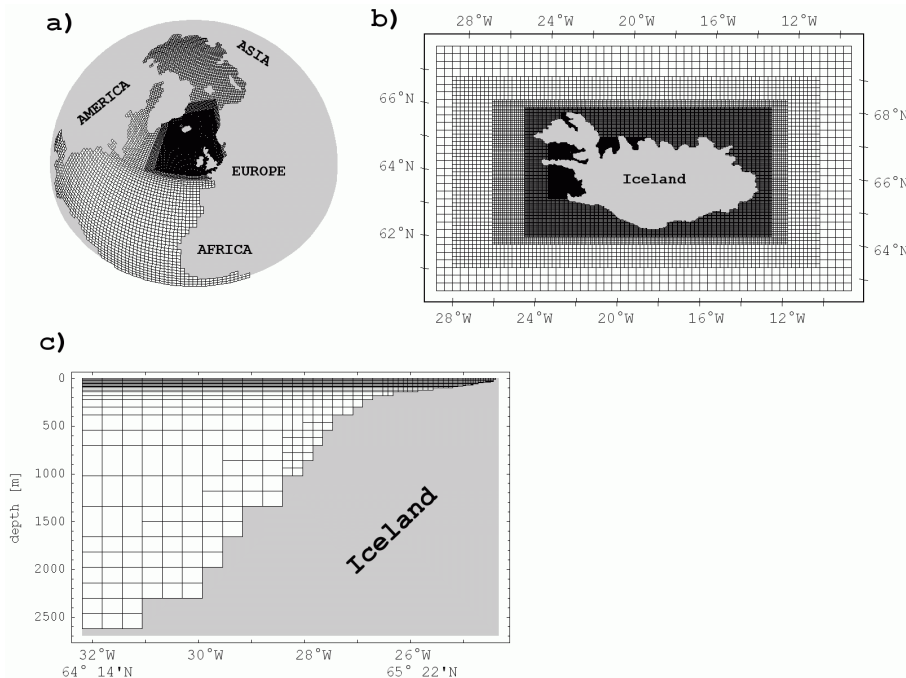


Fig. 4. The adapted model grid: **(a)** whole model domain including the North Atlantic, the Nordic Seas and the Arctic Ocean, **(b)** high resolution grid around Iceland, **(c)** section west of Iceland.

NIIC modelling

K. Logemann and
I. H. Harms

[Title Page](#)

[Abstract](#)

[Introduction](#)

[Conclusions](#)

[References](#)

[Tables](#)

[Figures](#)

[|◀](#)

[▶|](#)

[◀](#)

[▶](#)

[Back](#)

[Close](#)

[Full Screen / Esc](#)

[Printer-friendly Version](#)

[Interactive Discussion](#)

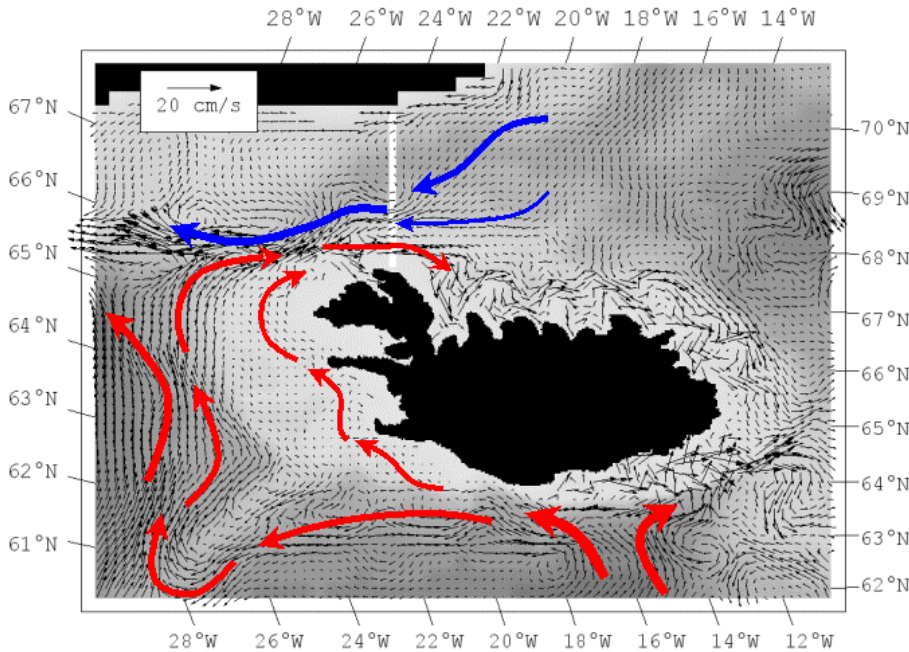


Fig. 5. Simulated mean velocity for the period 1997–2003 in 100 m depth. Scale refers to black arrows; coloured arrows are schematic.

NIIC modelling

K. Logemann and
I. H. Harms

[Title Page](#)

[Abstract](#)

[Introduction](#)

[Conclusions](#)

[References](#)

[Tables](#)

[Figures](#)

[◀](#)

[▶](#)

[◀](#)

[▶](#)

[Back](#)

[Close](#)

[Full Screen / Esc](#)

[Printer-friendly Version](#)

[Interactive Discussion](#)

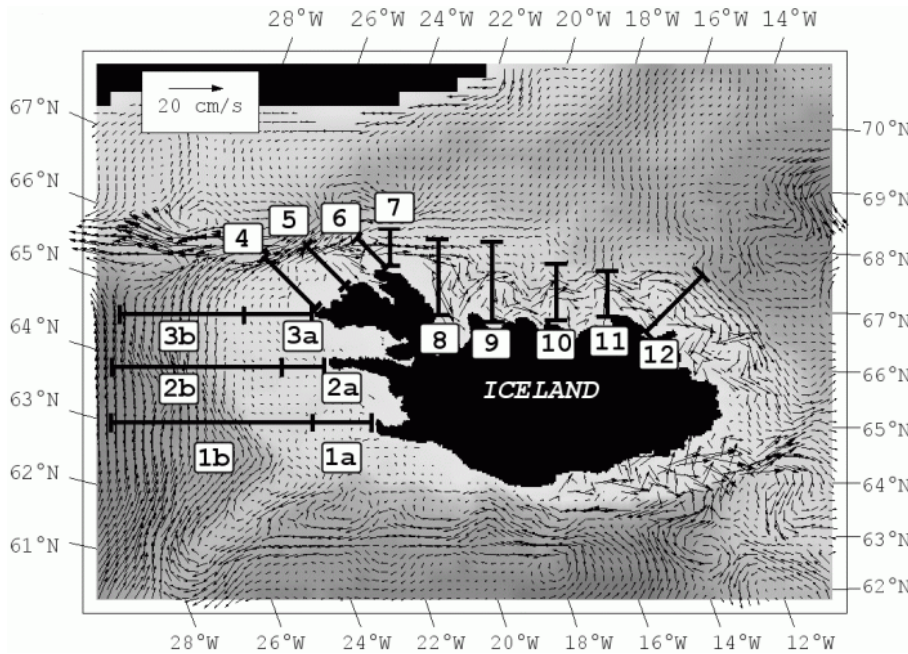


Fig. 6. Simulated mean velocity field at 100 m depth for the period 1997–2003 and positions of 15 analysed model sections (Table 2).

NIIC modelling

K. Logemann and
I. H. Harms

[Title Page](#)

[Abstract](#)

[Introduction](#)

[Conclusions](#)

[References](#)

[Tables](#)

[Figures](#)

[|◀](#)

[▶|](#)

[◀](#)

[▶](#)

[Back](#)

[Close](#)

[Full Screen / Esc](#)

[Printer-friendly Version](#)

[Interactive Discussion](#)

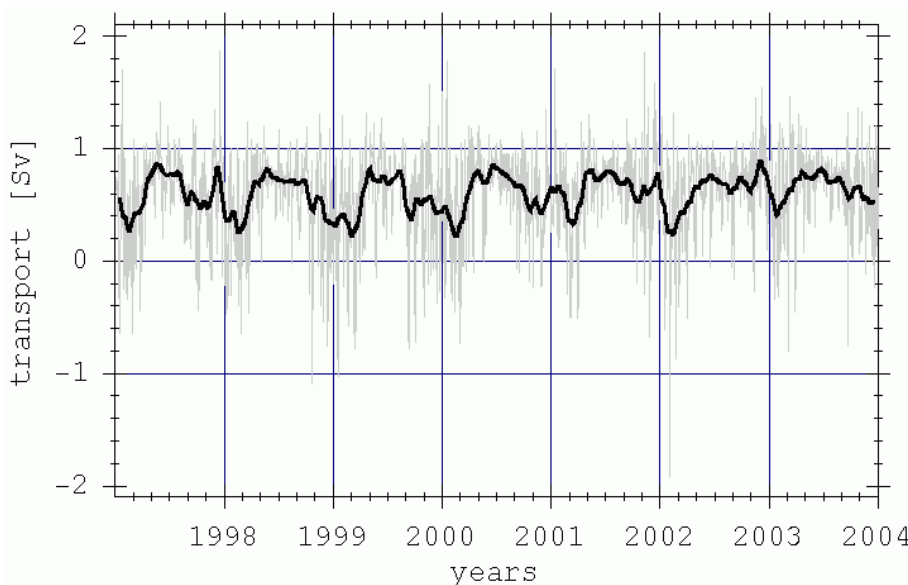


Fig. 7. Simulated eastward volume flux through section 7. The grey curve shows daily means, the black curve shows low pass filtered values with a cut-off frequency of $(20 \text{ days})^{-1}$.

NIIC modelling

K. Logemann and
I. H. Harms

[Title Page](#)

[Abstract](#)

[Introduction](#)

[Conclusions](#)

[References](#)

[Tables](#)

[Figures](#)

[◀](#)

[▶](#)

[◀](#)

[▶](#)

[Back](#)

[Close](#)

[Full Screen / Esc](#)

[Printer-friendly Version](#)

[Interactive Discussion](#)

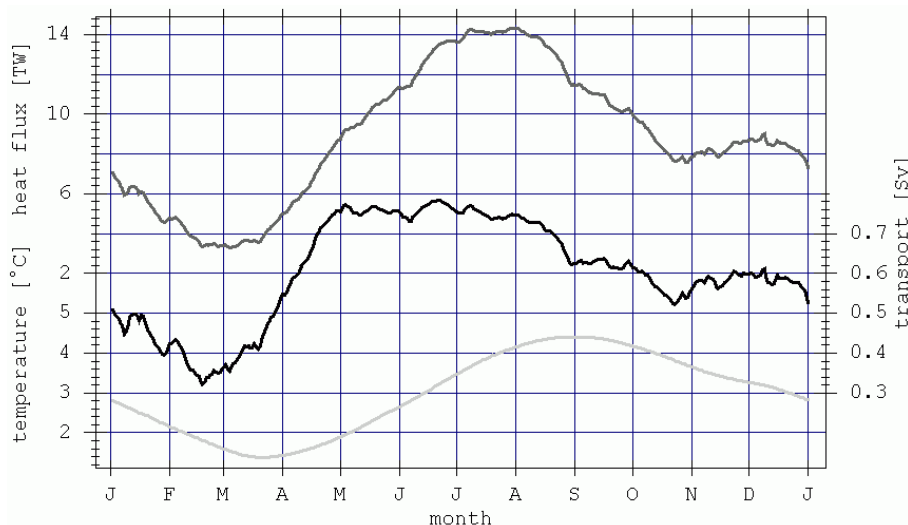


Fig. 8. Seasonal variability derived from the 1997–2003 simulation (31 days moving averages). Uppermost dark-grey curve: NIIC heat flux (relative to 0°C) at section 7; black curve: NIIC volume flux normal to section 7; light-grey curve: spatially averaged water temperature over the North Icelandic shelf (area between section 7 and 12 with water depth below 300 m).

NIIC modelling

K. Logemann and
I. H. Harms

[Title Page](#)

[Abstract](#)

[Introduction](#)

[Conclusions](#)

[References](#)

[Tables](#)

[Figures](#)

◀

▶

◀

▶

[Back](#)

[Close](#)

[Full Screen / Esc](#)

[Printer-friendly Version](#)

[Interactive Discussion](#)

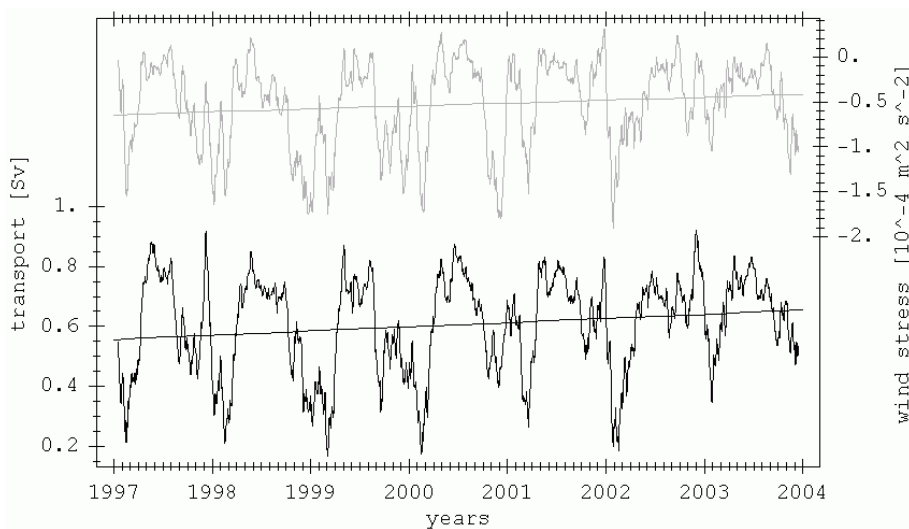


Fig. 9. 31 day moving averages of the northerly wind stress component (NCEP) (divided by the water density of 1030 kg m^{-3}) at $67^{\circ}40' \text{ N}$, $22^{\circ}32' \text{ W}$ (upper curve) and simulated volume flux of the NIIC normal to section 7 (lower curve). Trends 1997–2003 are: $3.2 \text{ } 10^{-6} \text{ m}^2 \text{ s}^{-2}$ per year for the wind stress, and 0.014 Sv per year for the volume flux.

NIIC modelling

K. Logemann and
I. H. Harms

[Title Page](#)

[Abstract](#)

[Introduction](#)

[Conclusions](#)

[References](#)

[Tables](#)

[Figures](#)

◀

▶

◀

▶

[Back](#)

[Close](#)

[Full Screen / Esc](#)

[Printer-friendly Version](#)

[Interactive Discussion](#)

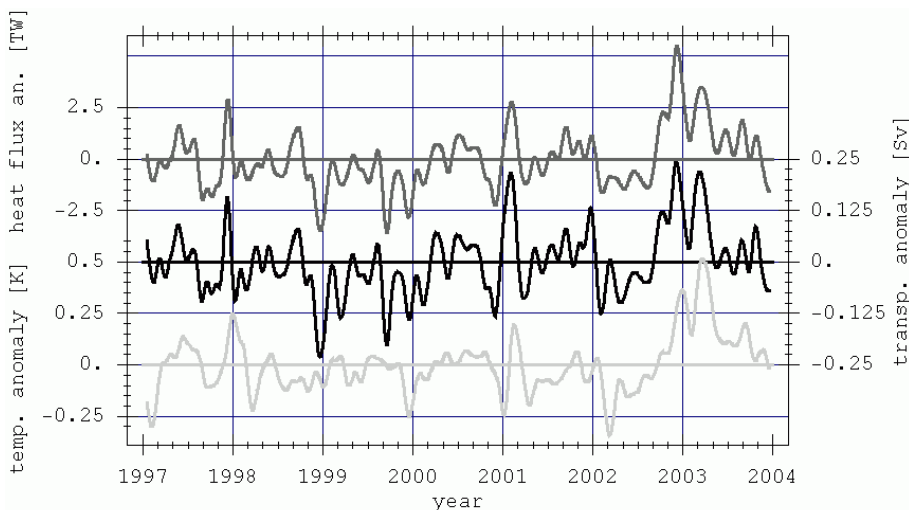


Fig. 10. Low-pass filtered (cut-off frequency: $(30 \text{ days})^{-1}$) anomalies relating to the seasonal signals shown in Fig. 8. The uppermost, dark-grey curve shows the NIIC's simulated heat flux anomalies at section 7. The black curve in the middle shows the NIIC's volume flux anomalies normal to section 7. The light-grey curve below shows the spatially averaged water temperature over the North Icelandic shelf (area between section 7 and 12 with water depth below 300 m).

NIIC modelling

K. Logemann and
I. H. Harms

[Title Page](#)

[Abstract](#)

[Introduction](#)

[Conclusions](#)

[References](#)

[Tables](#)

[Figures](#)

◀

▶

◀

▶

[Back](#)

[Close](#)

[Full Screen / Esc](#)

[Printer-friendly Version](#)

[Interactive Discussion](#)

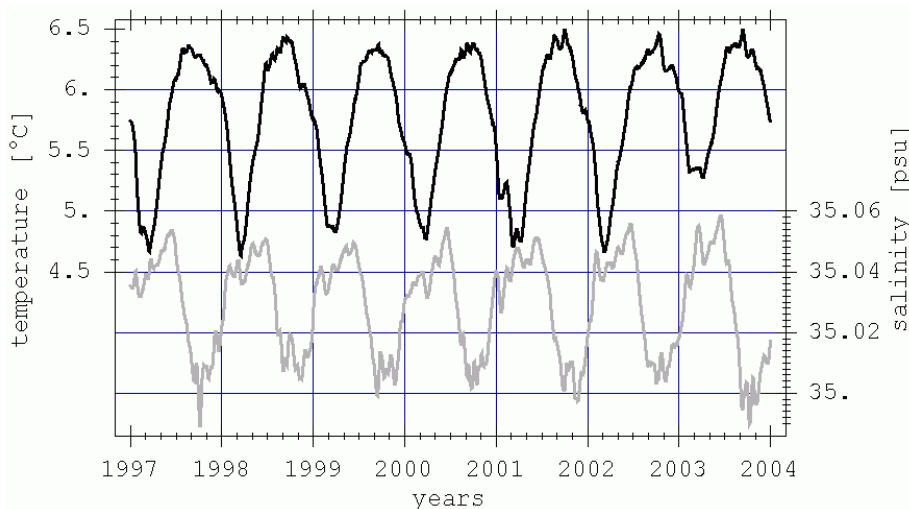


Fig. 11. Low-pass filtered (cut-off frequency: $(30 \text{ days})^{-1}$) simulated temperature (upper black curve) and salinity (lower grey curve) at section 3b (mean between surface and 800 m depth) south of Denmark Strait.

NIIC modelling

K. Logemann and
I. H. Harms

[Title Page](#)

[Abstract](#)

[Introduction](#)

[Conclusions](#)

[References](#)

[Tables](#)

[Figures](#)

◀

▶

◀

▶

[Back](#)

[Close](#)

[Full Screen / Esc](#)

[Printer-friendly Version](#)

[Interactive Discussion](#)

NIIC modelling

K. Logemann and
I. H. Harms

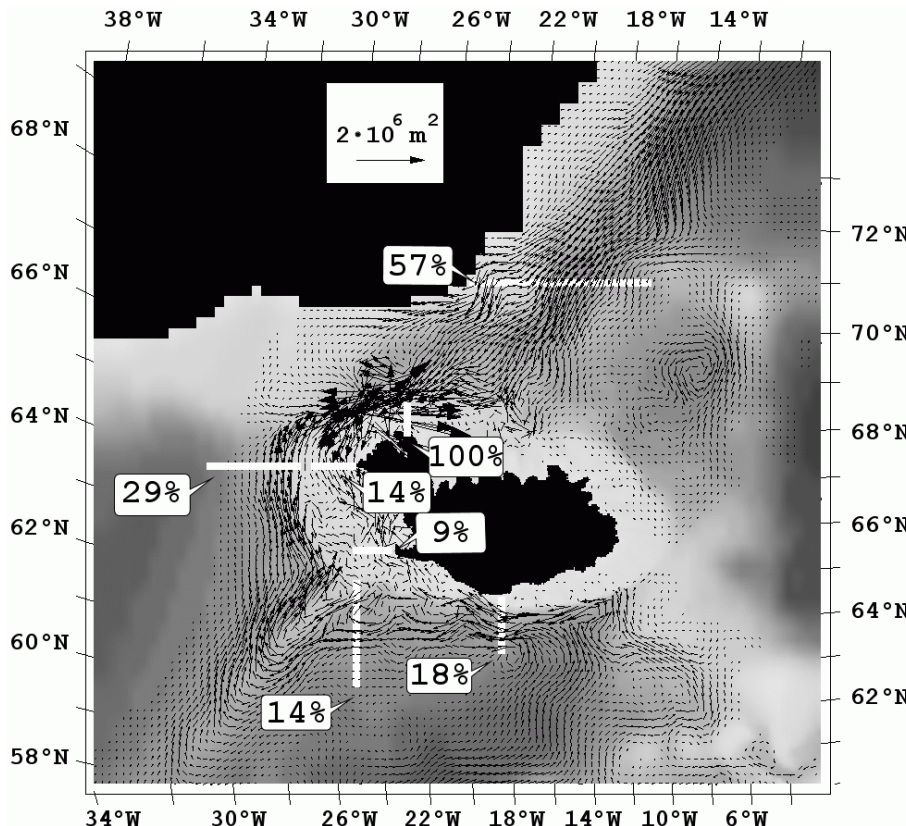


Fig. 12. Origins, pathways and composition of NIIC water masses. Vectors show the vertically integrated tracer flux over three years. The percentage values refer to the white sections and indicate the fraction of the initial volume (100%) that passed these sections during three years.

[Title Page](#)[Abstract](#)[Introduction](#)[Conclusions](#)[References](#)[Tables](#)[Figures](#)[|◀](#)[▶|](#)[◀](#)[▶](#)[Back](#)[Close](#)[Full Screen / Esc](#)[Printer-friendly Version](#)[Interactive Discussion](#)

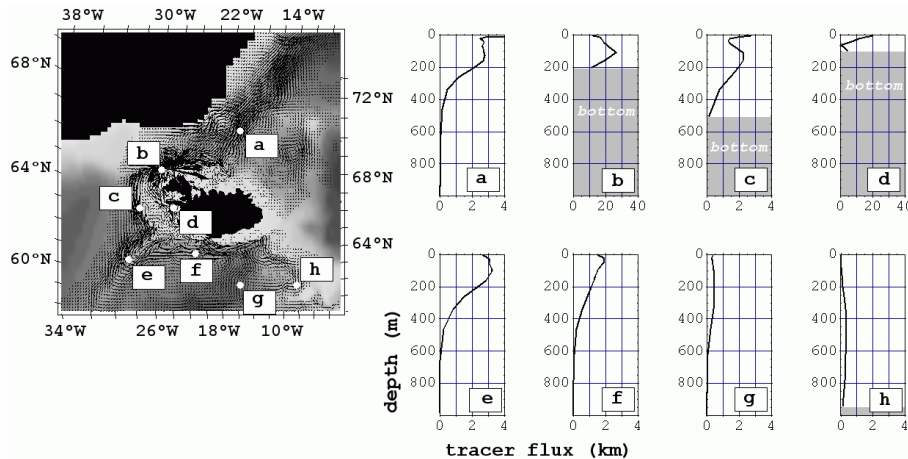


Fig. 13. Vertical profiles of NIIC tracer flux (c.f. Fig. 12) integrated over three years. Letters refer to the profile position. Note the higher range for profile b and d.

NIIC modelling

K. Logemann and
I. H. Harms

[Title Page](#)

[Abstract](#)

[Introduction](#)

[Conclusions](#)

[References](#)

[Tables](#)

[Figures](#)

[◀](#)

[▶](#)

[◀](#)

[▶](#)

[Back](#)

[Close](#)

[Full Screen / Esc](#)

[Printer-friendly Version](#)

[Interactive Discussion](#)

NIIC modelling

K. Logemann and
I. H. Harms

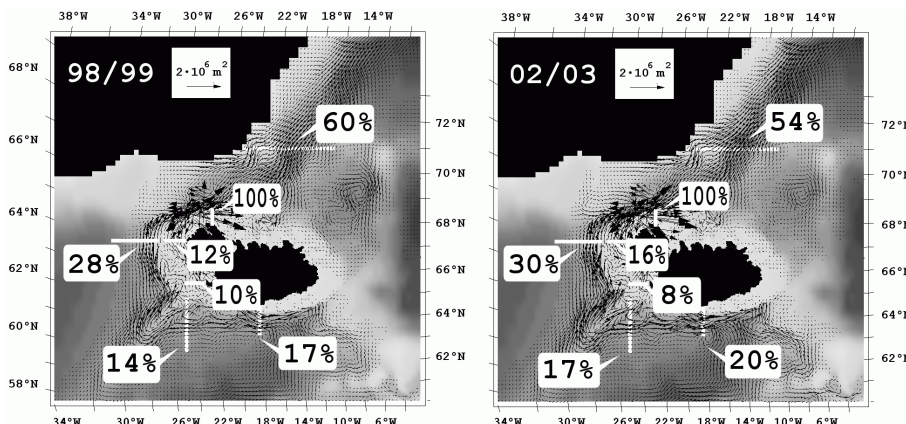


Fig. 14. Origins, pathways and composition of NIIC water masses. Repeated simulation of the NIIC tracer dispersion (c.f. Fig. 12) on the basis of two different current fields. Left: Mean current field October 1998–1999 (weak NIIC = 0.5 Sv at section 7). Right: Mean current field September 2002–2003 (strong NIIC = 0.7 Sv at section 7).

[Title Page](#)

[Abstract](#)

[Introduction](#)

[Conclusions](#)

[References](#)

[Tables](#)

[Figures](#)

◀

▶

◀

▶

[Back](#)

[Close](#)

[Full Screen / Esc](#)

[Printer-friendly Version](#)

[Interactive Discussion](#)

EGU

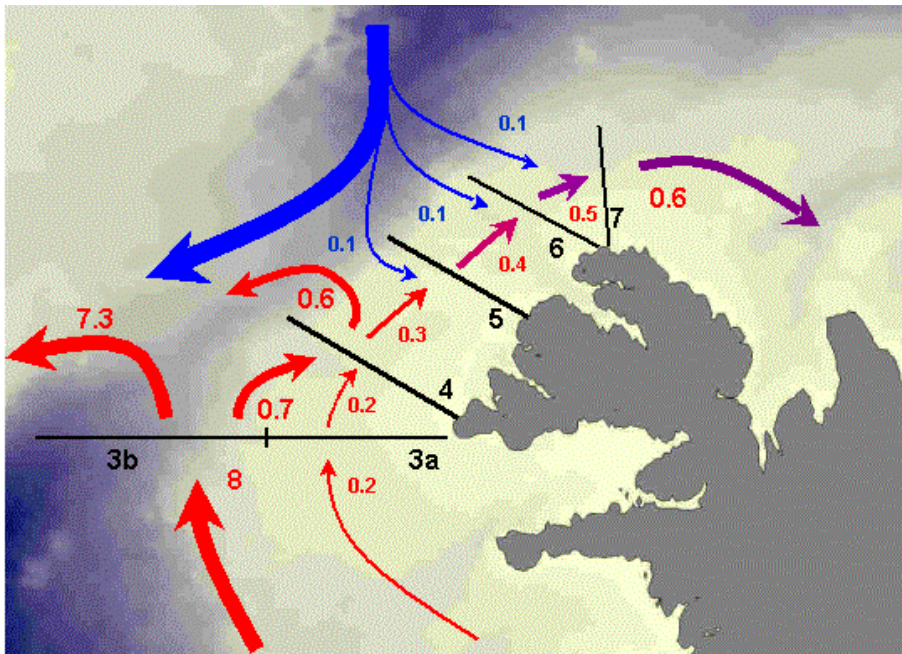


Fig. 15. Sketch of the NIIC pathway and volume flux based on climatological flow fields. Red AW contribution, blue PW contribution. Black numbers denote sections, coloured numbers are Sverdrup rates. Note that the 0.3 Sv AW continuing north beyond section 4 consist of 67% off-shore branch and 33% in-shore branch water, i.e. both branches are significantly reduced due to re-circulation to the west.

NIIC modelling

K. Logemann and
I. H. Harms

[Title Page](#)

[Abstract](#)

[Introduction](#)

[Conclusions](#)

[References](#)

[Tables](#)

[Figures](#)

[|◀](#)

[▶|](#)

[◀](#)

[▶](#)

[Back](#)

[Close](#)

[Full Screen / Esc](#)

[Printer-friendly Version](#)

[Interactive Discussion](#)

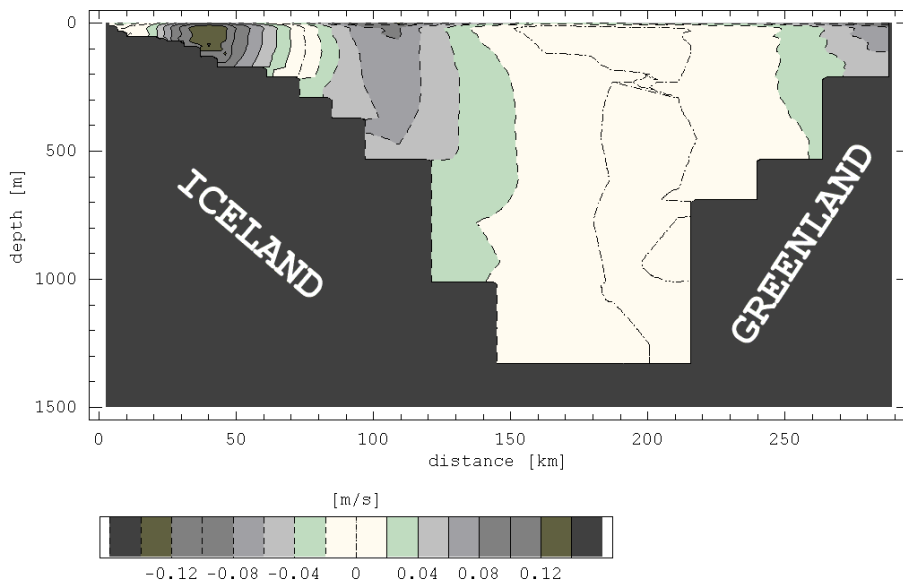


Fig. 16. Cross-section flow in Denmark Strait (white line in Fig. 5). Negative (positive) values indicate south-westward (north-eastward) flow.

NIIC modelling

K. Logemann and
I. H. Harms

[Title Page](#)

[Abstract](#)

[Introduction](#)

[Conclusions](#)

[References](#)

[Tables](#)

[Figures](#)

◀

▶

◀

▶

[Back](#)

[Close](#)

[Full Screen / Esc](#)

[Printer-friendly Version](#)

[Interactive Discussion](#)

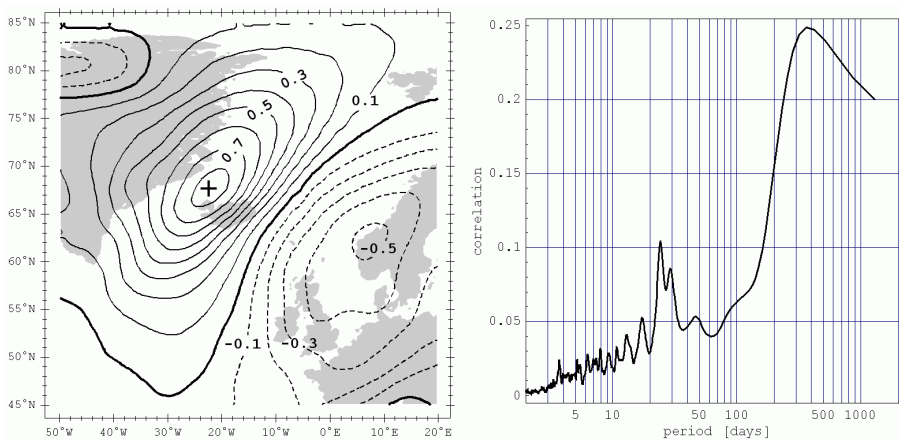


Fig. 17. Correlation coefficients between the north component of the daily mean wind stress and the volume flux of the NIIC, normal to section 7 (left). The maximum coefficient is 0.857, north-west of Iceland at $67^{\circ}40' \text{N}, 22^{\circ}32' \text{W}$ (cross). Right figure shows the cross spectrum of the correlation between both time series at this position. Highest correlation is found at a period of a year (seasonal cycle), other maxima at periods of 24 and 29 days.

NIIC modelling

K. Logemann and
I. H. Harms

[Title Page](#)

[Abstract](#)

[Introduction](#)

[Conclusions](#)

[References](#)

[Tables](#)

[Figures](#)

◀

▶

◀

▶

[Back](#)

[Close](#)

[Full Screen / Esc](#)

[Printer-friendly Version](#)

[Interactive Discussion](#)